Magnetic Resonance in Medicine 64:1499–1509 (2010)

Assessment of Multiexponential Diffusion Features as MRI Cancer Therapy Response Metrics

Benjamin A. Hoff,[1] Thomas L. Chenevert,[1] Mahaveer S. Bhojani,[2] Thomas C. Kwee,[1] Alnawaz Rehemtulla,[2] Denis Le Bihan,[3] Brian D. Ross,[1] and Craig J. Galbán[1]*

The aim of this study was to empirically test the effect of chemotherapy-induced tissue changes in a glioma model as measured by several diffusion indices calculated from nonmonoexponential formalisms over a wide range of *b*-values. We also compared these results to the conventional two-point apparent diffusion coefficient calculation using nominal *b*-values. Diffusion-weighted imaging was performed over an extended range of *b*-values (120–4000 sec/mm^2) on intracerebral rat 9L gliomas before and after a single dose of 1,3-bis(2-chloroethyl)-1-nitrosourea. Diffusion indices from three formalisms of diffusion-weighted signal decay [(a) two-point analytical calculation using either low or high *b*-values, (b) a stretched exponential formalism, and (c) a biexponential fit] were tested for responsiveness to therapy-induced differences between control and treated groups. Diffusion indices sensitive to "fast diffusion" produced the largest response to treatment, which resulted in significant differences between groups. These trends were not observed for "slow diffusion" indices. Although the highest rate of response was observed from the biexponential formalism, this was not found to be significantly different from the conventional monoexponential apparent diffusion coefficient method. In conclusion, parameters from the more complicated nonmonoexponential formalisms did not provide additional sensitivity to treatment response in this glioma model beyond that observed from the two-point conventional monoexponential apparent diffusion coefficient method. Magn Reson Med 64:1499–1509, 2010. ©2010 Wiley-Liss, Inc.

Key words: diffusion weighted-MRI; multiexponential diffusion; glioma; treatment response; preclinical

Diffusion-weighted magnetic resonance imaging (DWI) shows promise as an imaging biomarker for treatment response in glioma patients (1–9) as well as in a variety of other clinical tumor types (10–16). Routine in almost all preclinical and clinical scanners, diffusion maps can be generated from a minimum of two images acquired at low (*b*-value $\sim$ 100 sec/mm^2) and high (*b*-value $\sim$ 1000 sec/mm^2) diffusion weightings. Assuming monoexponential signal attenuation with *b*-value, the apparent diffusion coefficient (ADC) can be calculated analytically. The application of diffusion MRI for the detection of early tumor treatment response was first reported using a rodent glioma model using diffusion weightings at nominal *b*-values ($\leq$1000 sec/mm^2) (17). This initial report has been verified and expanded by ensuing publications using different tumor models and therapeutic agents (1,18,19), supporting the use of diffusion MRI as a sensitive imaging biomarker capable of detecting early cellular changes in treated tumors which precede macroscopic volumetric response.

The efficacy of this technique lies in its sensitivity to the molecular motion of water, which is affected by cellular, subcellular, and macromolecular elements that impede otherwise free diffusion of water. Thus, therapeutic changes within the tumor at the cellular level can be monitored by serial diffusion measurements (20–23). Through thermal random motion, water molecules sample the surrounding microarchitecture within tissues at length scales (few microns) much smaller than typical MRI voxel resolution ($\sim$millimeter). The theoretical basis for diffusion analysis is that cell membranes and other structures hinder the diffusion of molecules (20,24). The magnitude of diffusion-driven displacement is altered by tortuosity and hindering effects and can therefore be used to infer their presence and density. Studies have revealed that in biological systems water proton signal attenuation due to diffusion weighting does not follow monoexponential decay, and the deviation from monoexponential behavior is best observed at relatively high *b*-values ($\geq$3000 sec/mm^2). A more accurate description of signal attenuation with *b*-value over this wide *b*-value range requires more complex biophysical models (25–28).

An early interpretation of multiexponential diffusion patterns was that water moves within two or more compartments representing pools of "fast" (extracellular) and "slow" (intracellular) diffusion components in the signal. At low *b*-values the "fast" diffusion pool dominates signal attenuation, whereas at high *b*-values the "slow" diffusion pool dominates leading to a biexponential form for signal decay. Biexponential signal attenuation in DWI has been studied extensively in a variety of biological systems, and the physical mechanisms that govern nonmonoexponential decay continue to be an area of debate. An alternative formalism for the nonmonoexponential decay incorporates the underlying complexity in the diffusion medium as a continuous distribution of diffusion coefficients arising from a multiplicity of pools. Termed the "stretched-exponential" formalism, Bennett et al. (29) provided an analytical representation of the signal attenuation as a function of the probability density with a particular diffusion coefficient. Although this

[1]Department of Radiology, Center for Molecular Imaging, University of Michigan, Ann Arbor, Michigan, USA.

[2]Department of Radiation Oncology, Center for Molecular Imaging, University of Michigan, Ann Arbor, Michigan, USA.

[3]NeuroSpin, CEA Saclay, France.

Grant sponsor: National Institutes of Health; Grant numbers: P01CA85878, U24CA83099, and P50CA93990.

*Correspondence to: Craig J. Galbán, Ph.D., Assistant Professor, Radiology Department, University of Michigan, BSRB, Room D206, 109 Zina Pitcher Place, Ann Arbor, MI 48109-2200. E-mail: cgalban@med.umich.edu

Received 18 August 2009; revised 24 March 2010; accepted 20 April 2010.

DOI 10.1002/mrm.22507

Published online 21 September 2010 in Wiley Online Library (wileyonlinelibrary.com).

formalism can be used to infer the intravoxel diffusion heterogeneity within a biological system, it does not lend itself to straightforward association between biophysical compartments and signal decay. Although the "stretched-exponential" formalism has not been evaluated for its sensitivity to treatment response in tumors, this method has shown promise for characterizing tumors in brain cancer patients (30,31).

Research investigating the sensitivity of high *b*-value DWI for treatment assessment has shown promising results (5,32). Mardor et al. have demonstrated in patients with malignant brain lesions that the ratio of the diffusion coefficient from the "fast" pool and the "slow" pool signal fraction is highly sensitive to radiation-induced changes in the tumor. This parameter not only demonstrated a significant change from baseline as early as 1 week post-treatment initiation but was capable of predicting clinical outcome in all of the studied patients (5). In contrast, conventional monoexponential ADC (in their study, low and high *b*-values were 120 and 1200 sec/mm^2, respectively) was found to be predictive of outcome in only half of the patient population studied. Sensitivity of high *b*-value DWI to treatment was also observed in a colon cancer mouse model (32). These authors used the area under the normalized nonmonoexponential diffusion curve to quantify the diffusion characteristics of the tissue. This diffusion index was found to provide early prognostic information on animal responsiveness to treatment.

In this study, three nonmonoexponential diffusion formalisms applied over an extended range of *b*-values (120–4000 sec/mm^2) were tested against the conventional two-point ADC measurement to determine their sensitivity to therapy-induced changes of tissue using a rodent brain tumor model. Results showed similar time response curves for all diffusion indices following treatment. Although the highest fractional change following treatment was observed using the biexponential formalism, these results were not significantly different from those observed using the conventional two-point ADC calculation.

MATERIALS AND METHODS

Animal Tumor Models

9L gliosarcoma cells were obtained from the Brain Tumor Research Center at the University of California in San Francisco. The cells were grown as monolayers in 10 cm^2 sterile plastic flasks in DMEM with 10% fetal bovine serum, 100 IU/mL penicillin, 100 mg/mL streptomycin, and 2 mmol/L L-glutamine in an incubator held at 37°C and 95%/5% air/CO_2 atmosphere. Before implantation, cells were harvested by trypsinization, counted, and resuspended in serum-free medium for injection.

Tumor implantation was performed on Male Fischer 344 rats (Harlan Sprague-Dawley, Indianapolis, IN), weighing ~125–150 g, as previously described (33). Briefly, animals were anesthetized with a ketamine/xylazine mixture (87/13 mg/kg) administered intraperitoneal. A small incision was then made over the right hemisphere of the cranium. A 1 mm diameter burr hole was drilled through the skull using a high-speed surgical drill, and a 5 μL suspension containing 1×10^5 9L cells was injected through the burr hole to a depth of 3 mm. After injection of the cells, the burr hole was filled with bone wax to prevent extracranial extension of the tumor, and the surgical area was cleaned using 70% ethanol. Vetbond (3M, St. Paul, MN) was used to close the incision until healed.

Chemotherapy

Once the tumors reached 40–80 mm^3 as quantified using T_2-weighted MRI, pretreatment diffusion-weighted (DW) images (details below) were acquired for all animals. At the time of treatment, 1,3-bis(2-chloroethyl)-1-nitrosourea (BCNU) (LKT Laboratories, St. Paul, MN) was freshly prepared and formulated to a final concentration of 5 mg/mL BCNU in 10% ethanol. Subsequent to their pretreatment DWI scan, animals either received a single bolus intraperitoneal injection of BCNU (9.98 mg/kg; $n = 13$) or 10% ethanol as the control vehicle ($n = 10$). Typically, tumors increased in volume by 400% over the duration of the study (2 weeks post-treatment initiation), and euthanasia was accomplished by CO_2 overdose.

MRI Scans

During MRI examinations, animals were anesthetized with 1–2% isoflurane/air, and body temperature was maintained by blowing warm air through the bore of the magnet using an Air-Therm (World Precision Instruments, Sarasota, FL). MR scans were performed immediately before treatment and every 3 days thereafter using a 9.4 T, 16 cm horizontal bore Varian (Palo Alto, CA) Direct Drive system with a quadrature rat head coil (Doty Scientific, Inc., Columbia, SC). DW images were acquired using a spin-echo sequence, with a navigator echo and gradient waveforms sensitive to isotropic diffusion (34), with the following parameters: repetition time (TR)/echo time (TE) = 4000/41 msec, field of view (FOV) = 30 mm, matrix size = 64 × 64, slice thickness = 2 mm, number of slices = 8, sweep width = 50 kHz, gradient pulse width = 10.5 msec, gradient pulse separation = 25 msec, and *b*-values (*x*-gradient, *y*-gradient, and *z*-gradient amplitudes) of 120 (5.3, 4.8, and 4.2 G/cm), 1200 (16.6, 15.0, and 13.1 G/cm), 1600 (19.1, 17.3, and 15.6 G/cm), 2000 (21.3, 19.2, and 17.4 G/cm), 3000 (25.9, 23.4, and 21.3 G/cm), and 4000 sec/mm^2 (29.7, 26.9, and 24.6 G/cm) with averages of 1, 1, 1, 1, 4, and 16, respectively. DWI scans were constrained to a total scan time of 2 h based upon an institutionally approved animal protocol. In addition to the time constraint, only voxels in the tumor with a signal to noise (SNR) > 6 at high diffusion weighting (i.e., $b = 4000$ sec/mm^2) were evaluated. The first step in maintaining this constraint was to determine a voxel size that provides adequate SNR and resolution within a 2 h MR experiment. As observed in Chenevert et al. (3), 9L rodent brain tumors treated with 13.3 mg/kg BCNU can exhibit an ADC as high as 1.5×10^{-3} mm^2/sec. A sucrose phantom of 15% sucrose/water, with a measured ADC of 1.4×10^{-3} mm^2/sec over the $b = 120$–1200 sec/mm^2 range, was used to determine sequence

parameters (i.e., FOV, slice thickness, and averages) that provide a SNR > 6 at $b = 4000$ sec/mm^2 (35).

Postprocessing of Diffusion-Weighted Images

All MRI data were transferred to a PC, interpolated to a matrix size of 256 × 256, and analyzed using in-house software developed in MATLAB (The MathWorks, Inc., Natick, MA). Diffusion signal decay, found to follow a nonmonoexponential trend in healthy brain tissue and tumor from our animal model, was analyzed using three diffusion approaches.

Two-Point Analytical Formalism

The simplest of all three techniques investigated captures the nonmonoexponential trends observed in the DW images from a two-point subsampling of the signal decay curve using the following equation:

$$\mathrm{ADC}_{1-2} = \ln\left(\frac{S_1}{S_2}\right)\Big/(b_2 - b_1), \qquad [1]$$

where S_1 and S_2 are the signal intensities at b-values b_1 and b_2, respectively, and ADC_{1-2} is the diffusion coefficient obtained using b_1 and b_2. The conventional monoexponential ADC was calculated using b-values of 120 and 1200 sec/mm^2 ($\mathrm{ADC}_{120-1200}$), which captures the rapid diffusion decay in the nominal-b regime while avoiding perfusion effects observed at very low b-value (<100 sec/mm^2). Slow diffusion decay, observed in the high-b regime, was captured by determining the ADC using b-values of 2000 and 4000 sec/mm^2 ($\mathrm{ADC}_{2000-4000}$). The ratio of $\mathrm{ADC}_{2000-4000}/\mathrm{ADC}_{120-1200}$, defined as R_{TP}, was used as an empiric index of nonmonoexponential behavior derived from the piece-wise two-point formalism. An R_{TP} close to one implies monoexponential behavior, whereas a decreasing R_{TP} implies greater disparity in signal decay between low-b and high-b regimes, thus greater multiexponential behavior.

Stretched Exponential Formalism

This formalism defines the divergence of a diffusible particle from monoexponential trends as anomalous diffusion (29,36). Referred to as the stretched exponential, this formalism portrays molecular diffusion in a locally nonhomogeneous environment, which is represented by the equation:

$$S(b) = S_0[e^{-(b\cdot\mathrm{DDC})^{\alpha}}], \qquad [2]$$

where S is the signal intensity at a given b-value, S_0 is the signal intensity with no diffusion weighting, DDC is the distributed diffusion coefficient, and α is the anomalous exponent bound between 0 and 1 (29,36). By inspection of Eq. 2, it should be clear an $\alpha = 1$ is equivalent to monoexponential diffusion signal decay. Conversely, an α approaching 0 indicates a high degree of multiexponential signal decay, thus α will be used as the nonmonoexponential index derived from the stretched exponential formalism. This convention maintains consistency with Bennett et al.'s (29) definition of α as a diffusion heterogeneity index, although we remind the reader that a numerically high α value (~1) represents a low intravoxel diffusion heterogeneity approaching monoexponential decay, whereas a numerically low α value represents a high degree of diffusion heterogeneity exhibited as multiexponential decay. It is also worth emphasis that the term "heterogeneity" in this context refers to intravoxel heterogeneity of exponential decays, as opposed to intervoxel heterogeneity of diffusion coefficients as often is the case, particularly in tumor. Parameter maps of DDC and α were calculated by linearizing the stretched exponential equation and then fitting it to the DW images in a pixel-wise manner over all b-values using a linear least-squares technique.

Biexponential Model

Calculation of the biexponential diffusion components was performed by a pixel-wise fit to all DW images of the following equation:

$$S(b) = S_0\left(V_1 e^{(-bD_1)} + V_2 e^{(-bD_2)}\right) \qquad [3]$$

where S and S_0 are signal intensities at a given b-value and no diffusion weighting, respectively, D_1 and D_2 are the fast and slow diffusion coefficients, respectively, and V_1 and V_2 are the fast and slow signal fraction contributions, respectively. The fractional signal components are related by the expression $V_2 = 1 - V_1$. The fit was performed using a nonlinear least-squares technique.

Image Analysis

Volumes of interest (VOI) over the tumors were manually contoured on the low b-value DWI, which exhibits T_2-weighted contrast and serves for quantification of tumor volume. Low SNR voxels were excluded before calculation of mean parameter values within the VOI from each diffusion formalism. To accomplish this, voxels having SNR ≤ 6 on the $b = 4000$ sec/mm^2 DWI were identified by software in a binary 3D mask. The mask was then applied to all DW images guaranteeing that only those voxels with a SNR > 6 were evaluated. Regions of necrosis or blood pools, typically observed as hypointense on T_2-weighted images, were manually omitted from the VOIs. Parameter change with respect to treatment was assessed using the percent change of the mean of each parameter (100×[Posttherapy − Pretherapy]/Pretherapy).

Histology

An additional six animals were used for obtaining histology of the tumors for control ($n = 3$) and treated animals ($n = 3$) 6 days post-treatment. 9L tumors from these animals were placed in buffered formalin overnight, dehydrated in 70% ethanol, and subsequently embedded in paraffin. Tissue sections were prepared for histological processing by routine techniques. Briefly, paraffin sections (5 μm thick) were cut on a microtome and heated for 20 min at 65°C. Slides were deparaffinized in xylene with three changes for 5 min each and then rehydrated through an alcohol gradient for 2 min each (100% alcohol, 95% alcohol, and 70% alcohol). Sections were first

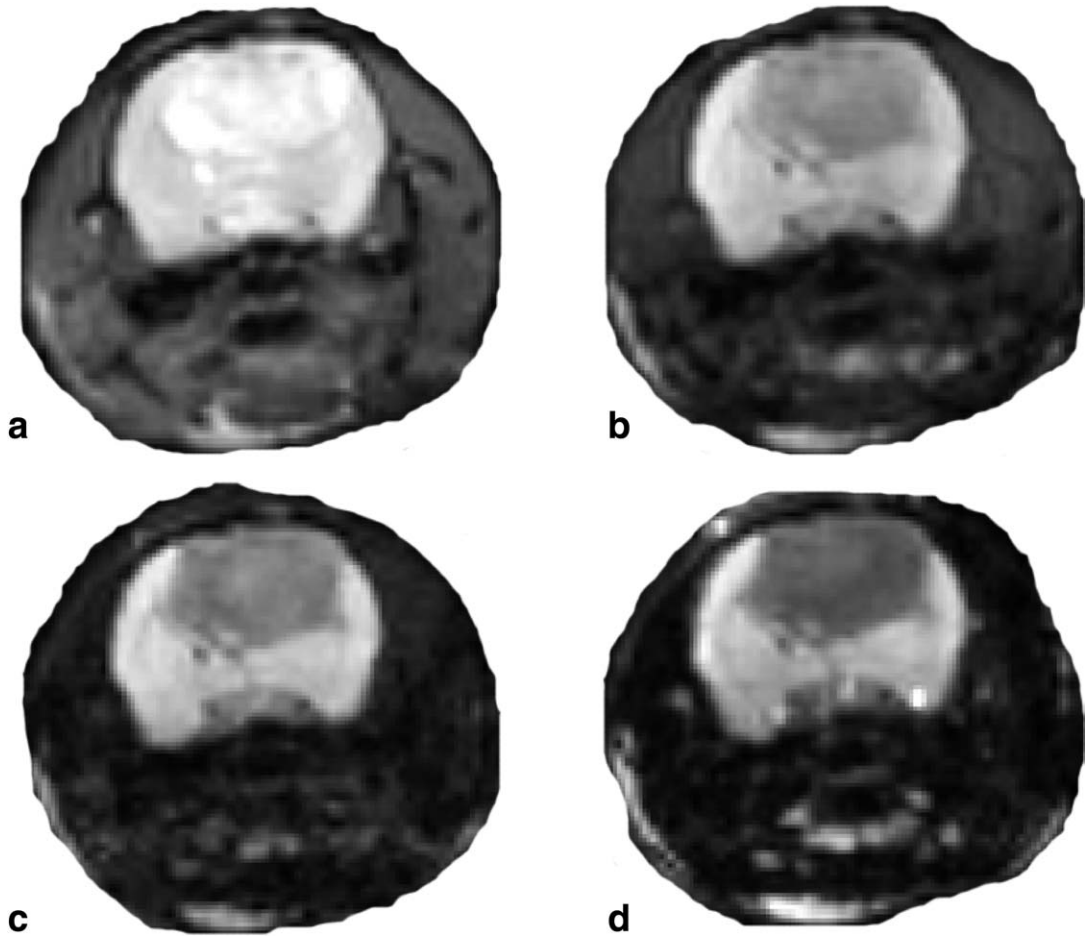

FIG. 1. Representative diffusion-weighted images of a rat brain harboring a 9L gliosarcoma acquired at *b*-values of (**a**) 120, (**b**) 1200, (**c**) 2000, and (**d**) 4000 sec/mm^2. Images were independently scaled for better visualization at higher *b*-values.

stained using a Gill's 2× hematoxylin solution and then subsequently stained with eosin.

Statistics

A paired Student's *t*-test was used to assess significance between the percent change in each parameter post-treatment initiation from pretreatment values and between the percent change in similar parameters for each formalism at individual time points in the treated group. Group comparisons were assessed for each parameter at individual time points using an independent sample Student's *t*-test. Treatment efficacy on overall survival was assessed by log-rank test and displayed using a Kaplan-Meier survival curves. All statistical computations were performed with a statistical software package (SPSS Software Products, Chicago, IL). Statistical significance was assessed at $P < 0.05$.

RESULTS

Representative DW images, acquired at *b*-values of 120, 1200, 3000, and 4000 sec/mm^2, are demonstrated in Fig. 1. Using low *b*-value images, delineation of tumor extent allowed for tumor volumes to be measured over time. Although the tumor volume in treated animals did appear to have a slower rate of growth than controls, this did not result in statistical differences in tumor volume between groups at individual time points (Fig. 2a). Nevertheless, as presented in Fig. 2b, the median survival of treated animals (9 days with a 95% confidence interval of 8.2–9.8 days) was found to be significantly longer than control animals (5 days with a 95% confidence interval of 3.8–6.2 days; $P = 0.001$). Increased longevity in treated animals was consequent to tumor cell death, which was verified by histology. Histological sections of representative control and treated animals at day 6 post-treatment initiation are presented in Fig. 3. Following BCNU treatment, fewer nuclei were observed in the treated tumor than control, suggesting massive cell kill in the tumor volume of treated animals. An increase in pleomorphism and giant cells was also evident in the treated tumors. Tumor growth rate kinetics and histology were consistent with previous findings using the 9L gliosarcoma rat brain tumor model (5).

Presented in Table 1 is a summary of the parametric indices generated from the three formalisms for control and treated tumor groups acquired at baseline. Significant differences in indices with similar diffusion properties were observed between all formalisms. In contrast, group comparisons did not result in statistical differences for any given parameter (Table 1: parameter values

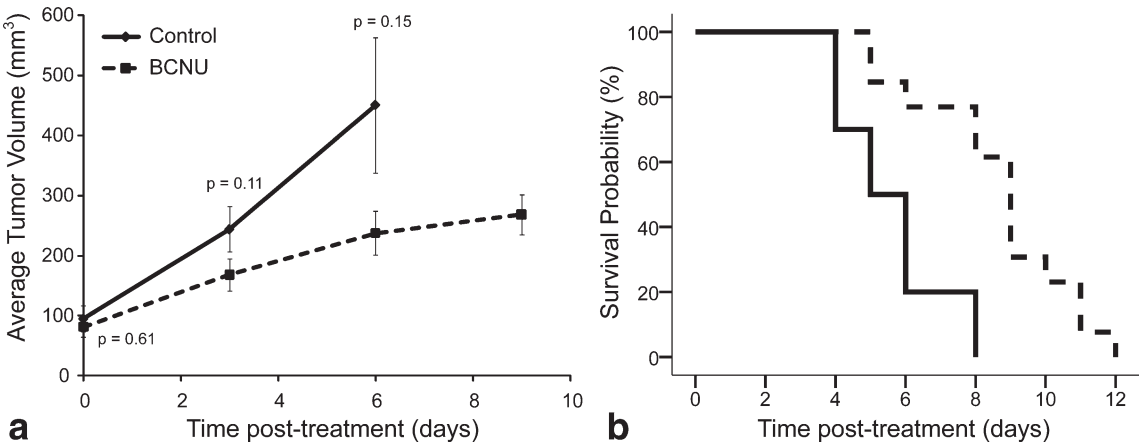

FIG. 2. **a**: Plot over time of the mean tumor volume. Data presented as mean ± SEM. Significant difference in mean tumor volume between groups was assessed using an unpaired Student's *t*-test. *P* values are provided at individual time points. **b**: Kaplan-Meier survival plot for overall survival is presented for control and treated animals. Controls are shown as solid line with diamond markers and treated are shown as dashed lines with square markers. Significant differences in overall survival were observed between groups as assessed using a log-rank test ($P = 0.001$).

for control and treated animals are summarized in the top and bottom rows, respectively). To verify the accuracy of our biexponential fit to the data, pretreatment values were calculated in healthy rat striatum. Biexponential results of D_1 and V_1 (0.88×10^{-3} mm^2/sec and 0.79) were found to be comparable with previous values

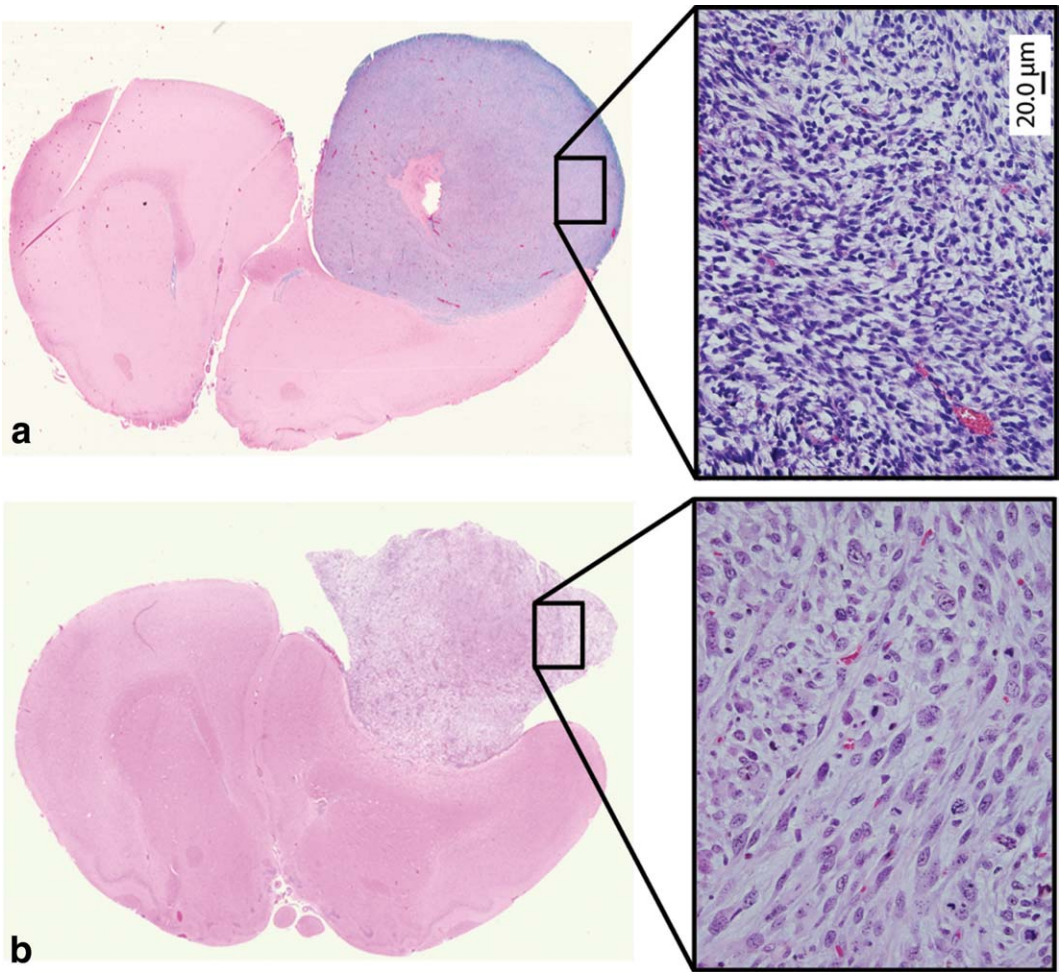

FIG. 3. Hematoxylin–eosin-stained sections of intracerebral 9L tumors for representative (**a**) control and (**b**) BCNU-treated animals on day 6 post-treatment.

Table 1
Mean Parameter Values at Baseline

Two-Point	Stretched exponential	Biexponential
$ADC_{120-200}$ [$\times 10^{-2}$ mm^2/sec].	DDC [$\times 10^{-3}$ mm^2/sec]	D_1 [$\times 10^{-3}$ mm^2/sec]
1.02 (0.02)	0.97 (0.02)	1.39 (0.05)
0.99 (0.03)	0.95 (0.02)	1.38 (0.05)
$ADC_{2000-1000}$ [$\times 10^{-3}$ mm^2/sec]		D_2 [$\times 10^{-3}$ mm^2/sec]
0.71 (0.02)		0.68 (0.03)
0.69 (0.01)		0.62 (0.02)
R_{TP}	α	V_2
0.71 (0.02)	0.83 (0.01)	0.39 (0.01)[a]
0.71 (0.02)	0.87 (0.01)	0.35 (0.01)[a]
$ADC_{120-200}/R_{TP}$	DDC/α	D_1N_2
1.46 (0.07)	1.10 (0.04)	3.99 (0.18)
1.48 (0.05)	1.09 (0.03)	3.74 (0.19)

Pretreatment data are presented for controls (n = 10; top) and treated (n = 13; bottom) animals as means (SEM).
[a]The slow fractional signal intensity is provided because of similar trends to R_{TP} and α post-treatment initiation.

in brain tissue (28). In contrast, D_2 (0.42 $\times$ 10^{-3} mm^2/sec) was 2.5$\times$ that of Niendorf et al.'s measurement of 0.165 $\times$ 10^{-3} mm^2/sec (28).

As shown in Fig. 4, maps of parameters more sensitive to "fast diffusion" properties pretreatment (left column) and 6 days following BCNU treatment (right column)

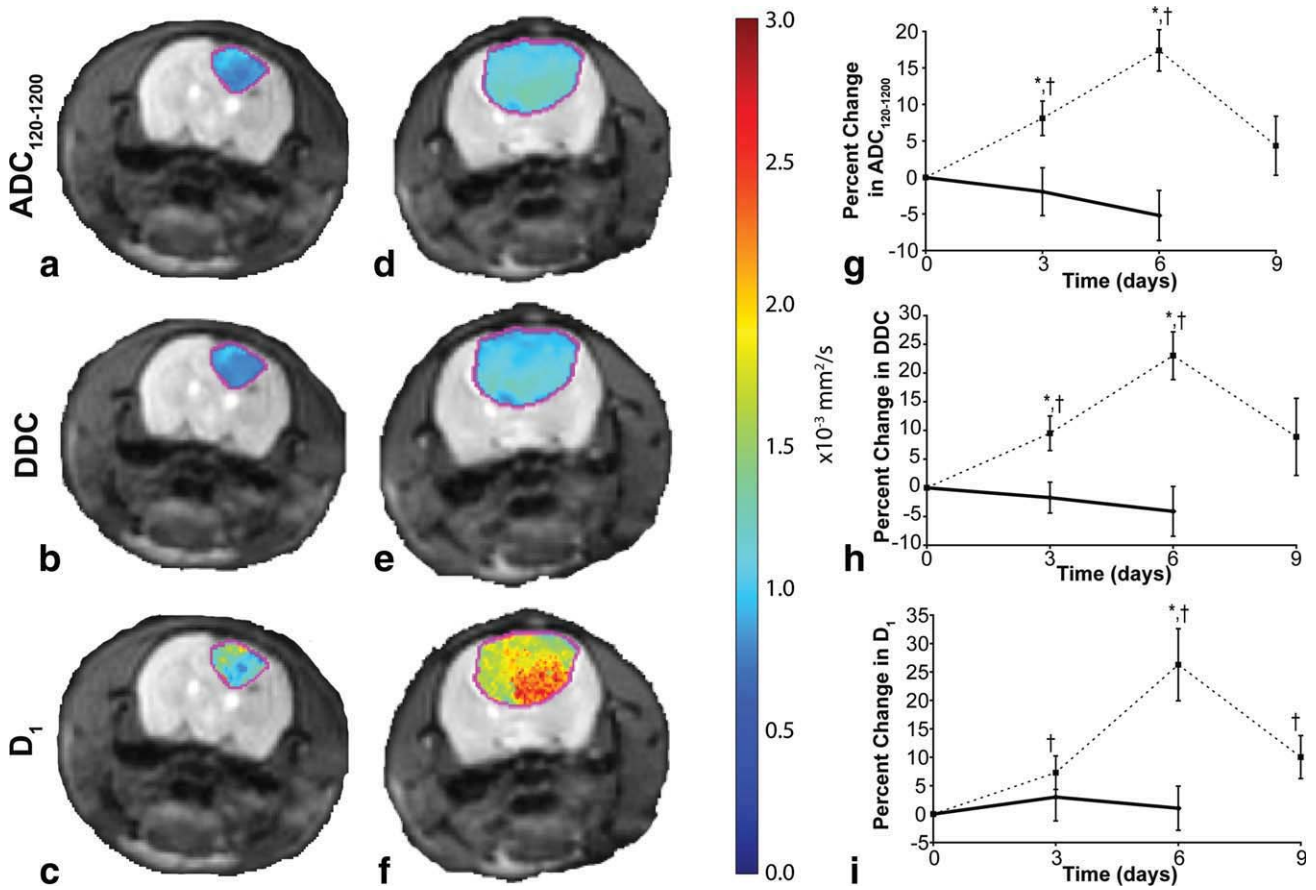

FIG. 4. Representative maps and line plots of percent change in parameters sensitive to "fast diffusion" generated using (**a**, **d**, **g**) two-point, (**b**, **e**, **h**) stretched-exponential, and (**c**, **f**, **i**) biexponential formalisms are provided. Diffusion maps, overlaid on T_2-weighted images of a rat brain, were acquired at days 0 (**a, b, c**) and 6 (**d, e, f**) post-treatment initiation. Line plots (**g, h, i**) consist of mean values and standard errors from control and treated groups over the entire experiment. Data are presented as the mean $\pm$ the standard error of the mean. The symbols † and * designate significant differences from baseline and between groups, respectively. Statistical significance was assessed at $P < 0.05$. [Color figure can be viewed in the online issue, which is available at wileyonlinelibrary.com.]

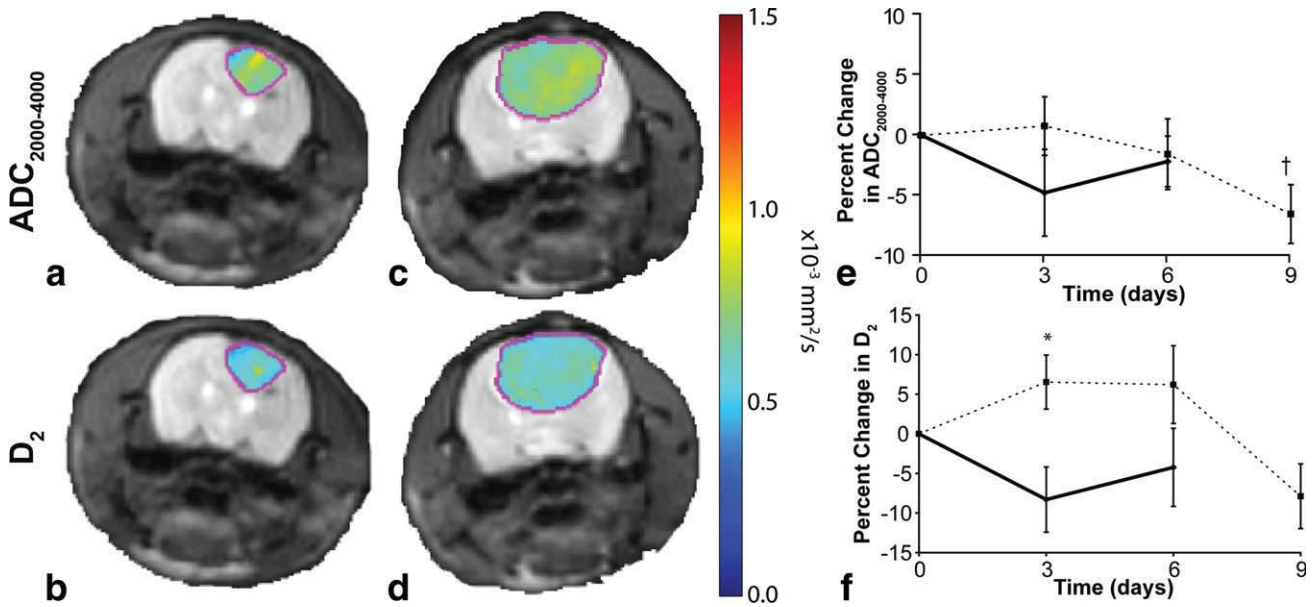

FIG. 5. Representative maps of the "slow diffusion" coefficients and line plots of percentage change in parameters generated using (**a**, **c**, **e**) two-point and (**b**, **d**, **f**) biexponential formalisms are provided. Diffusion maps, overlaid on T_2-weighted images of a rat brain, were acquired at days 0 (**a, b**) and 6 (**c, d**) post-treatment initiation. Line plots (**e, f**) consist of mean values and standard errors from control and treated groups over the entire experiment. Data are presented as the mean ± the standard error of the mean. The symbols † and * designate significant differences from baseline and between groups, respectively. Statistical significance was assessed at $P < 0.05$. [Color figure can be viewed in the online issue, which is available at wileyonlinelibrary.com.]

were generated over the tumor volume and superimposed on T_2-weighted images. Top-row images (Fig. 4a,d) represent $ADC_{120–1200}$, middle-row images (Fig. 4b,e) are DDC, and bottom-row images (Fig. 4c,f) are D_1. In addition, the full time course of $ADC_{120–1200}$, DDC, and D_1 expressed as percent change from pretreatment values are illustrated in Fig. 4g–i, respectively. D_1 was found to be significantly larger than $ADC_{120–1200}$ and DDC at baseline (Table 1) and at day 6 post-treatment initiation as well as having, in absolute terms, a larger dynamic range (~1.5–3.0 × 10^{-3} mm^2/sec) within the tumor volume allowing easier visualization of tumor features (Fig. 4c,f). As for the responsiveness of these indices to treatment, the percent change from baseline peaked at day 6 post-treatment initiation, followed by a descent toward baseline at day 9 (Fig. 4g–i). Near identical trends were observed for $ADC_{120–1200}$ and DDC with significant group and baseline value differences observed on days 3 and 6. Similar results were observed for D_1 except for the negligible group differences at day 3 post-treatment initiation, which is attributed to the slower rate of ascent from baseline (Fig. 4i). Although change in D_1 was found to be most responsive to treatment with a ~25% increase at day 6 from baseline, it was not found to be significantly larger at this time point or any other time point from what was observed for change in $ADC_{120–1200}$ and DDC ($P = 0.204$ and $P = 0.711$, respectively, for day 6).

Analogous parametric maps and line plots to Fig. 4 are illustrated in Fig. 5 for quantities sensitive to the "slow diffusion" component of the decay curve, namely $ADC_{2000–4000}$ (Fig. 5a,c,e) and D_2 (Fig. 5b,d,f). In general, $ADC_{2000–4000}$ and D_2 showed little change in day 6 values from baseline (Fig. 5a–d). Percent change in the mean values over time corroborates observations found in the maps from the representative animal (Fig. 5a–d) with $ADC_{2000–4000}$ and D_2 peaking at less than 10% of baseline. Group differences were only observed at day 3 for D_2, partly attributed to a drop in control D_2. Interestingly, both $ADC_{2000–4000}$ and D_2 resulted in ~7% decrease from baseline on day 9 post-treatment initiation (Fig. 5h,i), which correlated with the descent back to pretreatment values observed in diffusion coefficients sensitive to "fast diffusion" (Fig. 4).

As discussed previously, a comparison of the absolute numerical value of nonmonoexponential metrics is not meaningful because of differences in how these parameters are defined. Qualitatively, R_{TP} was most sensitive to treatment exhibiting the largest percent drop from baseline values (Fig. 6). The remaining parameters showed similar qualitative trends from baseline to day 6 post-treatment initiation. A significant drop from pretreatment values was observed at day 6 for R_{TP} (−11%), α (−7%), and V_2 (−6%). R_{TP} and α continued to have significantly lower values to baseline at day 9, which was not established by V_2 because of scatter in the data. Group differences were only found at day 6 for R_{TP} and α. The ratio of D_2 and D_1, as obtained from the biexponential formalism, provided analogous results to R_{TP} (data not shown). Although the mean value of D_2/D_1 decreased by more than 15%, these results were not found to be statistically different from the controls.

DISCUSSION AND CONCLUSIONS

DW MRI has shown potential as a surrogate biomarker for treatment response in cancer patients (37–40). Acquisition of diffusion maps is typically performed at

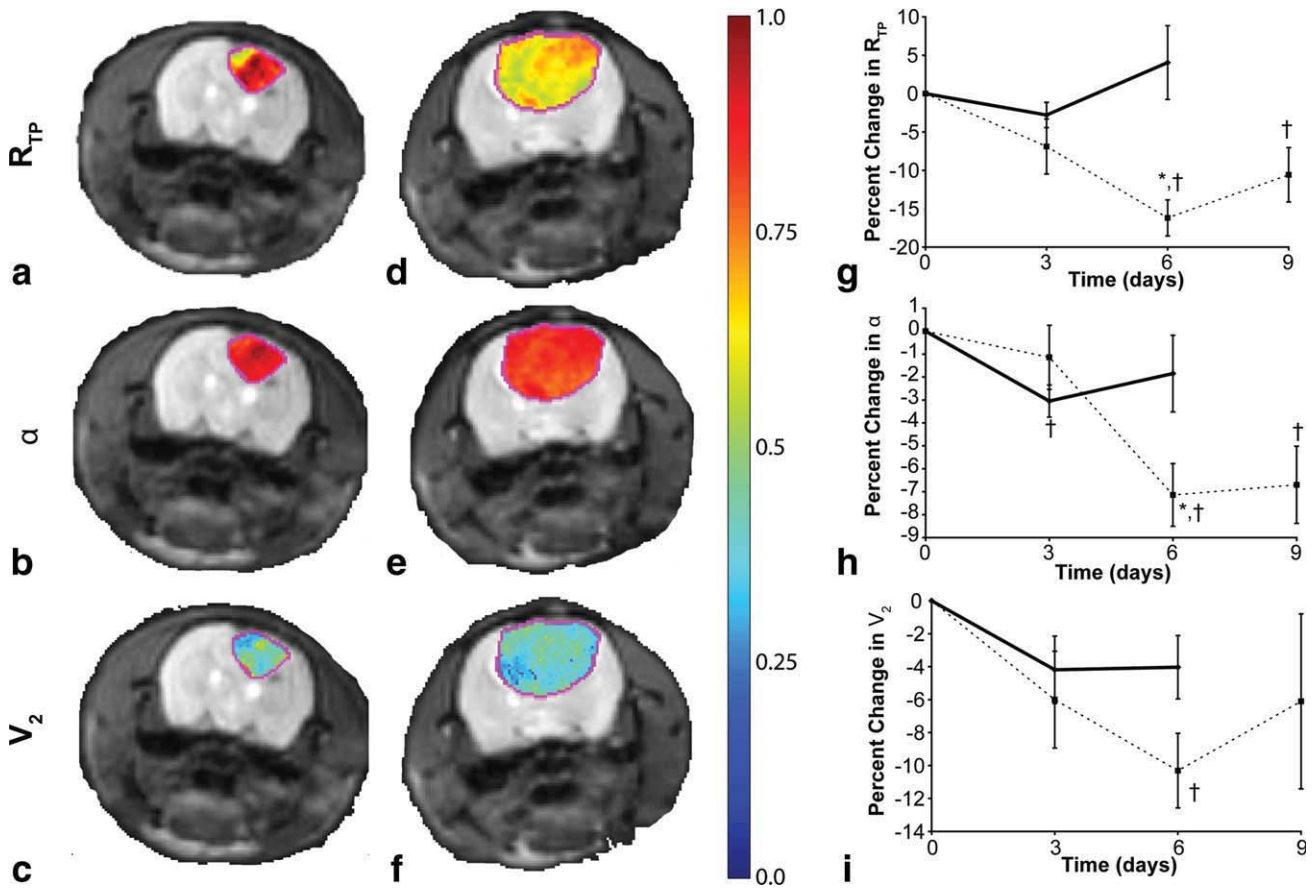

FIG. 6. Representative nonmonoexponential metric maps and line plots of percentage change in parameters generated using (**a**, **d**, **g**) two-point, (**b**, **e**, **h**) stretched-exponential, and (**c**, **f**, **i**) biexponential formalisms are provided. Metric maps, overlaid on T_2-weighted images of a rat brain, were acquired at days 0 (**a, b, c**) and 6 (**d, e, f**) post-treatment initiation. Line plots (**g, h, i**) consist of mean values and standard errors from control and treated groups over the entire experiment. Data are presented as the mean ± the standard error of the mean. The symbols † and * designate significant differences from baseline and between groups, respectively. Statistical significance was assessed at $P < 0.05$. [Color figure can be viewed in the online issue, which is available at wileyonlinelibrary.com.]

relatively moderate diffusion weighting, i.e., *b*-values that typically span the 0–1000 sec/mm^2 range. It is speculated that water diffusion measurements at higher *b*-values may provide increased sensitivity to relevant drug-induced changes in tumor composition by virtue of possible therapeutic alteration of cellular constituents responsible for the "slow diffusion" components of signal decay observed at relatively high *b*-values. This study sought to determine the sensitivity of diffusion parameters derived from various mathematical formalisms of nonmonoexponential water diffusion to treatment-induced tissue alteration following treatment of the 9L glioma model.

Previous work by our group using the 9L brain tumor model has shown that ADC calculated using moderate *b*-values can increase by up to 60% within a week following a single dose (13.3 mg/kg) of BCNU (3). As measured in this study, parameters sensitive to "fast diffusion" showed similar trends following a single bolus (9.98 mg/kg) of BCNU, all peaking by day 6 post-treatment initiation. The maximum percent change in parameter value from baseline was observed in D_1. This is expected because D_1 is a more specific measurement of "fast diffusion" than DDC and $ADC_{120–1200}$, which are not completely devoid of the "slow diffusion" properties in the signal decay curve. A positive therapeutic effect was confirmed by an increased overall survival (Fig. 2) as well as direct evidence from histological tumor sections comparing treated versus untreated tumors (Fig. 3). Another characteristic trend of ADC following treatment, which has been observed here and by others, is the temporally evolving descent to baseline values. This has been found to correlate with tumor cell repopulation, which has been reported in the literature (28). In contrast, those indices specifically sensitive to "slow diffusion" exhibited a negligible change post-treatment initiation until day 9 where a drop had occurred in both parameter values when compared with baseline. The lack of response following treatment and the sudden drop in $ADC_{2000–4000}$ and D_2 during cell repopulation, which is reflected in the diffusion coefficients sensitive to "fast diffusion" descent to baseline, is quite perplexing, suggesting independent mechanisms affecting the "fast" and "slow" diffusion properties of the tissue. Additional mechanisms, such as macrophage infiltration and clearance of macromolecules, may also contribute to our observations. Despite subtle variations in the trends of the parameters with either "fast" or "slow" diffusion

properties, there was no significant difference in the percent change from baseline between diffusion parameters with like properties.

As opposed to the diffusion coefficients, the nonmonoexponential metrics, R_{TP}, α, and V_2, are defined differently and thus cannot have the same interpretation, even though they have similar trends. Consequent to the negligible change in $ADC_{2000–4000}$, R_{TP} is driven almost exclusively by $ADC_{120–1200}$ for most of the study. Not until day 9, did we see a divergence from this dependence, which is partly attributed to the mirrored descent observed in $ADC_{2000–4000}$ to $ADC_{120–1200}$ resulting in a negligible change in R_{TP} from day 6 to day 9 post-treatment initiation. Analogous but not significant results were observed for D_2/D_1. Large variability in the measurement of D_1 and D_2 (Figs. 4 and 5) from the nonlinear fit most likely contributed to the nonstatistical differences in D_2/D_1 between groups. In contrast, the slow diffusion signal fraction, V_2, defines the proportion of water signal in the slow compartment independent of water diffusivity. The drop in V_2 suggests shrinkage of the slow compartment volume fraction, conversely an expansion of the fast compartment volume fraction, following treatment initiation. The anomalous exponent α represents the deviation of signal attenuation from monoexponential behavior ($\alpha = 1$). This perturbation is assumed to be attributed to increased heterogeneity within the tissue. The decrease in α seen in Fig. 6h suggests an increase in tumor intravoxel heterogeneity that maximizes at day 6 and continues to day 9. Following treatment of the tumor with BCNU, a loss in tumor cellularity (Fig. 3) further deviated the attenuation curve away from monoexponential behavior than what was observed from control and baseline values (Table 1). Because of similar trends in the nonmonoexponential metrics and the lack of response to treatment of the "slow diffusion" indices, one may speculate that the "fast diffusion" properties within the tumor dominate what we observe for R_{TP}, α, and V_2 following treatment. Various theories have been proposed to provide a physical account of the deviation in diffusion-sensitive signal attenuation from monoexponential behavior in biological tissue (20,21,41). Use of these theories to determine the exact physical properties that govern nonmonoexponential water diffusion warrants further investigation but is beyond the scope of this study.

Irrespective of the mechanisms driving nonmonoexponential behavior in diffusion-sensitive signal attenuation, high *b*-value DWI provides additional advantages over conventional monoexponential ADC measurements that may provide a more sensitive biomarker for tumor treatment response and characterization. The conventional approach for measuring ADC, *b*-values around 1000 sec/mm^2, is hindered by the presence of highly diffuse tissue, such as cysts and necrotic areas, which may reside within or around the tumor volume adding increasing difficulty in localizing viable tumor. At higher *b*-values, these rapidly diffusing regions within tumors are essentially filtered out leaving only densely packed tumor that has lower ADC values. Recent research investigating the sensitivity of high *b*-value DWI for treatment assessment has shown promising results. Mardor et al. have demonstrated in patients with malignant brain lesions that the ratio of D_1 and V_2 [defined as R in Eq. 1 of Ref. 5] is highly sensitive to radiation-induced changes in the tumor. This parameter not only demonstrated a significant change from baseline as early as 1 week post-treatment initiation but was capable of predicting clinical outcome in all of the studied patients. In contrast, conventional monoexponential ADC (comparable to $ADC_{120–1200}$ in this study) was only capable of predicting response in about half of their patient population. It is not clear whether R, as presented by Mardor et al., is driven by D_1 or V_2, or if D_1 or V_2 alone would provide ample sensitivity to predict tumor response to treatment as this analysis was not provided in their study. We further evaluated the approach proposed by Mardor et al. (5) (D_1/V_2) using our data. The percentage change in D_1/V_2 from baseline was ~42% in the treated group at day 6 post-treatment, which was significantly different from controls [−2% ($P = 0.002$)]. Although, D_1/V_2 demonstrated a percentage change 1.6× greater than that generated by D_1, this increase was not statistically different ($P = 0.15$). The probable cause for the lack of significance was the additional scatter in the data as a result of the nonlinear fit. Unlike DWI at moderate *b*-values, acquisition of diffusion-sensitized signal at *b*-values of >2000 sec/mm^2 is not trivial. This is attributed to the exponential loss of signal due to increased attenuation at high *b*-values. As signal approaches the noise floor, artificial nonmonoexponential trends in the signal profile are observed, adversely affecting the slow diffusion measurements. To accommodate these losses, images must be acquired with sufficient SNR resulting in longer scan times, which may not result in patient compliance. Additional computational time is also required when fitting the biexponential formalism to the DWI data. In this study, ~30 min per dataset was required for the voxel-wise nonlinear fit. The stretched-exponential formalism does not suffer from this deficiency because it can be linearized and solved using an algebraic solution of the linear least squares. Numerically fitting two parameters for the stretched exponential model can also be more stable relative to fitting three parameters required by the biexponential model.

There are several limitations to our experimental approach that must be discussed. Scan time was limited to no more than 2 h. This in turn limited the signal averaging, i.e., SNR, and range and number of *b*-values used per scanning session. As discussed, large slice thicknesses and small matrix sizes were used to maintain our self-imposed constraint of SNR > 6. This likely resulted in unavoidable partial volume averaging in the tumor, which would be less with thinner slices. Another area of concern was the lack of sufficiently high *b*-values, which are most sensitive to "slow diffusion" rates. This could have possibly led to an overestimation of the D_2 in the biexponential fit. Using the mean D_1 and D_2 determined at day 6 post-treatment initiation, we found in treated tumor tissue (1.7×10^{-3} mm^2/sec and 0.6×10^{-3} mm^2/sec), less than 4% (exp(−2000*0.0017) ~3.3%) of the fast diffusion signal was still present at a *b*-value of 2000 sec/mm^2, whereas 29.9% of the slow diffusion component signal was still available. Finally, the biexponential

diffusion coefficients, D_1 and D_2, acquired here for healthy striatum varied by only a factor of 2, contrary to the factor of 5–10 typically observed in the literature. Based on the observations of biexponential diffusion in rodent models, D_1 as measured in this study is in accordance with literature results (0.88 here, compared to 0.82 and 0.77 $\times$ 10^{-3} mm^2/sec in the literature), whereas D_2 appears to be overestimated by a factor of 2 (0.43 here, compared to 0.17 and 0.18 $\times$ 10^{-3} mm^2/sec in the literature) (28,41). The discrepancy in D_2 is most probably due to the lack of sufficiently high *b*-values used in this study. Finally, the filtering of low SNR voxels from our whole-tumor analysis may have inadvertently removed necrotic regions in the tumor. Signal intensity within regions of high diffusivity or short T2 due to blood products is prone to have low signal at high *b*-value. As discussed earlier, the contribution of noise in our data was reduced by filtering voxels whose SNR < 6 on the highest weighted DWI (4000 sec/mm^2). This maintained voxels having high SNR at high *b*-values but removed regions of high diffusivity or low SNR (i.e., necrosis, cystic, and blood products) from the whole-tumor analysis. To avoid excessive loss of tumor volume while maintaining SNR ≥ 6, image matrix size and slice thickness were set to maintain adequate SNR at a cost of resolution. The volume fraction of tumor analyzed at days 6 and 9 post-treatment initiation in treated animals was 93.5% $\pm$ 11.3% and 94.5% $\pm$ 9.9% (means $\pm$ SD), respectively. Based on these values, filtering tumor regions that contribute to low SNR in DWI at high *b*-value did not result in excessive loss of tumor volume for our analysis in this study.

We have demonstrated the sensitivity of various non-monoexponential diffusion formalisms for monitoring early response to chemotherapeutic treatment for brain tumors in an animal model. The extent of the response varied, with the fast diffusion component of the biexponential formalism exhibiting the largest percent change from baseline than other diffusion coefficient; slightly more than was observed in the conventional monoexponential ADC and DDC measurements. However, for this 9L glioma model treated with a single dose of BCNU, the more complicated formalisms provided no additional sensitivity to treatment response over what was observed using conventional monoexponential ADC measured over the standard modest *b*-value range.

REFERENCES

1. Chenevert TL, McKeever PE, Ross BD. Monitoring early response of experimental brain tumors to therapy using diffusion magnetic resonance imaging. Clin Cancer Res 1997;3:1457–1466.
2. Chenevert TL, Meyer CR, Moffat BA, Rehemtulla A, Mukherji SK, Gebarski SS, Quint DJ, Robertson PL, Lawrence TS, Junck L, Taylor JM, Johnson TD, Dong Q, Muraszko KM, Brunberg JA, Ross BD. Diffusion MRI: a new strategy for assessment of cancer therapeutic efficacy. Mol Imaging 2002;1:336–343.
3. Chenevert TL, Stegman LD, Taylor JM, Robertson PL, Greenberg HS, Rehemtulla A, Ross BD. Diffusion magnetic resonance imaging: an early surrogate marker of therapeutic efficacy in brain tumors. J Natl Cancer Inst 2000;92:2029–2036.
4. Hall DE, Moffat BA, Stojanovska J, Johnson TD, Li Z, Hamstra DA, Rehemtulla A, Chenevert TL, Carter J, Pietronigro D, Ross BD. Therapeutic efficacy of DTI-015 using diffusion magnetic resonance imaging as an early surrogate marker. Clin Cancer Res 2004;10:7852–7859.
5. Mardor Y, Pfeffer R, Spiegelmann R, Roth Y, Maier SE, Nissim O, Berger R, Glicksman A, Baram J, Orenstein A, Cohen JS, Tichler T. Early detection of response to radiation therapy in patients with brain malignancies using conventional and high b-value diffusion-weighted magnetic resonance imaging. J Clin Oncol 2003;21:1094–1100.
6. Moffat BA, Chenevert TL, Lawrence TS, Meyer CR, Johnson TD, Dong Q, Tsien C, Mukherji S, Quint DJ, Gebarski SS, Robertson PL, Junck LR, Rehemtulla A, Ross BD. Functional diffusion map: a non-invasive MRI biomarker for early stratification of clinical brain tumor response. Proc Natl Acad Sci USA 2005;102:5524–5529.
7. Moffat BA, Chenevert TL, Meyer CR, McKeever PE, Hall DE, Hoff BA, Johnson TD, Rehemtulla A, Ross BD. The functional diffusion map: an imaging biomarker for the early prediction of cancer treatment outcome. Neoplasia 2006;8:259–267.
8. Ross BD, Moffat BA, Lawrence TS, Mukherji SK, Gebarski SS, Quint DJ, Johnson TD, Junck L, Robertson PL, Muraszko KM, Dong Q, Meyer CR, Bland PH, McConville P, Geng H, Rehemtulla A, Chenevert TL. Evaluation of cancer therapy using diffusion magnetic resonance imaging. Mol Cancer Ther 2003;2:581–587.
9. Hamstra DA, Galban CJ, Meyer CR, Johnson TD, Sundgren PC, Tsien C, Lawrence TS, Junck L, Ross DJ, Rehemtulla A, Ross BD, Chenevert TL. Functional diffusion map as an early imaging biomarker for high-grade glioma: correlation with conventional radiologic response and overall survival. J Clin Oncol 2008;26:3387–3394.
10. Jacobs MA, Herskovits EH, Kim HS. Uterine fibroids: diffusion-weighted MR imaging for monitoring therapy with focused ultrasound surgery—preliminary study. Radiology 2005;236:196–203.
11. Seierstad T, Folkvord S, Roe K, Flatmark K, Skretting A, Olsen DR. Early changes in apparent diffusion coefficient predict the quantitative antitumoral activity of capecitabine, oxaliplatin, and irradiation in HT29 xenografts in athymic nude mice. Neoplasia 2007;9:392–400.
12. Dudeck O, Zeile M, Pink D, Pech M, Tunn PU, Reichardt P, Ludwig WD, Hamm B. Diffusion-weighted magnetic resonance imaging allows monitoring of anticancer treatment effects in patients with soft-tissue sarcomas. J Magn Reson Imaging 2008;27:1109–1113.
13. Cui Y, Zhang XP, Sun YS, Tang L, Shen L. Apparent diffusion coefficient: potential imaging biomarker for prediction and early detection of response to chemotherapy in hepatic metastases. Radiology 2008;248:894–900.
14. Harry VN, Semple SI, Gilbert FJ, Parkin DE. Diffusion-weighted magnetic resonance imaging in the early detection of response to chemoradiation in cervical cancer. Gynecol Oncol 2008;111:213–220.
15. Pickles MD, Gibbs P, Lowry M, Turnbull LW. Diffusion changes precede size reduction in neoadjuvant treatment of breast cancer. Magn Reson Imaging 2006;24:843–847.
16. Byun WM, Shin SO, Chang Y, Lee SJ, Finsterbusch J, Frahm J. Diffusion-weighted MR imaging of metastatic disease of the spine: assessment of response to therapy. AJNR Am J Neuroradiol 2002;23:906–912.
17. Ross BD, Chenevert TL, Kim B, Ben-Joseph O. Magnetic resonance imaging and spectroscopy: application to experimental neuro-oncology. Q Magn Reson Biol Med 1994;1:89–106.
18. Galons JP, Altbach MI, Paine-Murrieta GD, Taylor CW, Gillies RJ. Early increases in breast tumor xenograft water mobility in response to paclitaxel therapy detected by non-invasive diffusion magnetic resonance imaging. Neoplasia 1999;1:113–117.
19. Zhao M, Pipe JG, Bonnett J, Evelhoch JL. Early detection of treatment response by diffusion-weighted 1H-NMR spectroscopy in a murine tumour in vivo. Br J Cancer 1996;73:61–64.
20. Le Bihan D. Molecular diffusion, tissue microdynamics and microstructure. NMR Biomed 1995;8:375–386.
21. Le Bihan D. The 'wet mind': water and functional neuroimaging. Phys Med Biol 2007;52:R57-R90.
22. Lee KC, Moffat BA, Schott AF, Layman R, Ellingworth S, Juliar R, Khan AP, Helvie M, Meyer CR, Chenevert TL, Rehemtulla A, Ross BD. Prospective early response imaging biomarker for neoadjuvant breast cancer chemotherapy. Clin Cancer Res 2007;13 (2 Part 1):443–450.
23. Torigian DA, Huang SS, Houseni M, Alavi A. Functional imaging of cancer with emphasis on molecular techniques. CA Cancer J Clin 2007;57:206–224.
24. Le Bihan D, Turner R, Douek P. Is water diffusion restricted in human brain white matter? An echo-planar NMR imaging study. Neuroreport 1993;4:887–890.

25. Clark CA, Le Bihan D. Water diffusion compartmentation and anisotropy at high b values in the human brain. Magn Reson Med 2000;44: 852–859.
26. Cohen Y, Assaf Y. High b-value q-space analyzed diffusion-weighted MRS and MRI in neuronal tissues—a technical review. NMR Biomed 2002;15:516–542.
27. Kiselev VG, Il'yasov KA. Is the "biexponential diffusion" biexponential? Magn Reson Med 2007;57:464–469.
28. Niendorf T, Dijkhuizen RM, Norris DG, van Lookeren Campagne M, Nicolay K. Biexponential diffusion attenuation in various states of brain tissue: implications for diffusion-weighted imaging. Magn Reson Med 1996;36:847–857.
29. Bennett KM, Schmainda KM, Bennett RT, Rowe DB, Lu H, Hyde JS. Characterization of continuously distributed cortical water diffusion rates with a stretched-exponential model. Magn Reson Med 2003;50: 727–734.
30. Kwee TC, Galban CJ, Tsien C, Junck L, Sundgren PC, Ivancevic MK, Johnson TD, Meyer CR, Rehemtulla A, Ross BD, Chenevert TL. Comparison of apparent diffusion coefficients and distributed diffusion coefficients in high-grade gliomas. J Magn Reson Imaging 2010;31: 531–537.
31. Kwee TC, Galban CJ, Tsien C, Junck L, Sundgren PC, Ivancevic MK, Johnson TD, Meyer CR, Rehemtulla A, Ross BD, Chenevert TL. Intravoxel water diffusion heterogeneity imaging of human high-grade gliomas. NMR Biomed 2010;23:179–187.
32. Roth Y, Tichler T, Kostenich G, Ruiz-Cabello J, Maier SE, Cohen JS, Orenstein A, Mardor Y. High-b-value diffusion-weighted MR imaging for pretreatment prediction and early monitoring of tumor response to therapy in mice. Radiology 2004;232:685–692.
33. Ross BD, Zhao YJ, Neal ER, Stegman LD, Ercolani M, Ben-Yoseph O, Chenevert TL. Contributions of cell kill and posttreatment tumor growth rates to the repopulation of intracerebral 9L tumors after chemotherapy: an MRI study. Proc Natl Acad Sci USA 1998;95: 7012–7017.
34. Moffat BA, Hall DE, Stojanovska J, McConville PJ, Moody JB, Chenevert TL, Rehemtulla A, Ross BD. Diffusion imaging for evaluation of tumor therapies in preclinical animal models. Magma 2004;17: 249–259.
35. Laubach HJ, Jakob PM, Loevblad KO, Baird AE, Bovo MP, Edelman RR, Warach S. A phantom for diffusion-weighted imaging of acute stroke. J Magn Reson Imaging 1998;8:1349–1354.
36. Hall MG, Barrick TR. From diffusion-weighted MRI to anomalous diffusion imaging. Magn Reson Med 2008;59:447–455.
37. Chenevert TL, Sundgren PC, Ross BD. Diffusion imaging: insight to cell status and cytoarchitecture. Neuroimaging Clin N Am 2006;16: 619–632, viii-ix.
38. Hamstra DA, Rehemtulla A, Ross BD. Diffusion magnetic resonance imaging: a biomarker for treatment response in oncology. J Clin Oncol 2007;25:4104–4109.
39. Lee KC, Bradley DA, Hussain M, Meyer CR, Chenevert TL, Jacobson JA, Johnson TD, Galban CJ, Rehemtulla A, Pienta KJ, Ross BD. A feasibility study evaluating the functional diffusion map as a predictive imaging biomarker for detection of treatment response in a patient with metastatic prostate cancer to the bone. Neoplasia 2007;9:1003–1011.
40. Padhani AR, Liu G, Koh DM, Chenevert TL, Thoeny HC, Takahara T, Dzik-Jurasz A, Ross BD, Van Cauteren M, Collins D, Hammoud DA, Rustin GJ, Taouli B, Choyke PL. Diffusion-weighted magnetic resonance imaging as a cancer biomarker: consensus and recommendations. Neoplasia 2009;11:102–125.
41. Schwarcz A, Bogner P, Meric P, Correze JL, Berente Z, Pal J, Gallyas F, Doczi T, Gillet B, Beloeil JC. The existence of biexponential signal decay in magnetic resonance diffusion-weighted imaging appears to be independent of compartmentalization. Magn Reson Med 2004;51:278–285.